INT. J. NUM. METH. HEAT FLUID FLOW, VOL. 6, 35–46 (1996)

AXISYMMETRIC LASER WELDING OF CERAMIC AND METALLIC MATERIALS: FINITE ELEMENT MODELLING

J. A. THOMAZIN, L. G. OLSON[1] AND J. W. HIRSCH

Department of Mechanical Engineering and Center for Electro-Optics, University of Nebraska-Lincoln Lincoln, NE 68588-0656

ABSTRACT

In this paper, finite element techniques are used to model laser spot welding of both metallic and ceramic materials. The materials modelled were aluminum and alumina, a typical ceramic. In the formulation, the steady state mass, momentum, and energy conservation equations are considered with surface tension and buoyancy forces driving the fluid flow. The results indicate that fluid flow must be considered in order to accurately model molten pool characteristics for ceramics since the coupling of fluid flow to heat flow is more important for ceramics than for metals.

KEY WORDS Laser welding Finite elements Ceramics

INTRODUCTION

Applications in the automative, electronic, and superconductive materials industries have helped fuel the dramatically increased research activity in ceramics over the last ten years. Among the research efforts are attempts to incorporate the use of lasers in fusion processes for ceramic to ceramic bonds and also in ceramic to metal bonds. Many factors influence the strength and durability of the joined parts including material properties, fluid flow in the molten pool and heat transfer.

Many researchers have tried to gain a deeper understanding of the processes occurring in the molten pool during bonding by experimental studies and numerical modelling, both on traditional arc welding processes and laser welding. Numerical modelling of spot welding and linear welding has been attempted in both two- and three-dimensional systems with the emphasis on metals welding. Often, simplifying assumptions such as the Boussinesq approximation (which assumes the fluid is incompressible except for the effects of variable density in the buoyancy force) are applied to the numerical model. While the Boussinesq approximation may be valid for small temperature gradients, the approximation may be inaccurate when large temperature gradients are present during welding.

One of the earliest attempts at understanding the welding process using finite difference techniques was presented by Oreper and Szekely[1]. They considered an idealized spot TIG (Tungsten-inert-gas) welding process and allowed for electromagnetic, buoyancy, and surface tension forces in the numerical model. They identified the dominant nondimensional parameters inherent in the governing equations and determined the effects each had upon the final weld. When surface tension gradients were neglected they found that a broadly distributed heat and current flux caused the electromagnetic and buoyancy forces to strongly affect the fluid flow field; yet, they were insignificant in affecting the thermal flow field. Conversely, sharply focused

0961–5539/96/030035–12$2.00

Received July 1994
Revised October 1994

heat and current fluxes produced strong electromagnetically driven fluid flows causing considerable changes in the weld pool shape.

In addition, they concluded that the surface tension gradients present during welding cause surface velocities which affect weld pool shape. In later papers, Oreper *et al.*[2,3,4] improved the computational grid and further explored dominate forces such as electromagnetic, surface tension and buoyancy forces in the welding process. Also, these later papers helped develop mathematical details for manipulating the governing equations in addition to examining both numerically and analytically the effects material properties have on the final solution.

Thompson and Szekely[5] improved the previous work of Oreper *et al.* by incorporating a deformed free surface into a two-dimensional welding model. This procedure enabled them to examine the role surface deformation and surface tension forces play in controlling weld penetration. Furthermore they found that, while a depressed free surface significantly changes the weld penetration profile, it modifies surface velocities by less than 10% when compared to a flat free surface. For all cases Szekely and his colleagues[1,2,3,4,5] simplified the governing equations by means of Boussinesq assumptions and solved the equations using finite difference methods on rectangular grids for various spacings.

Ramanan and Korpela[6] were interested in gaining a deeper understanding of thermocapillary convection in relation to its influence on welding operations. Using the Boussinesq approximation with a stream function finite difference scheme, they indicated the thermocapillary forces dominate buoyancy forces. Later, Ramanan and Korpela[7] re-consider the axisymmetric analysis of a spot arc-weld pool and emphasize the appropriate dimensionless groups and numerical accuracy. Their numerical model utilized the Boussinesq approximation and assumed constant material properties. They indicate the mesh must be significantly refined near the free surface to resolve the velocity boundary layer.

Kou and Sun[8] began their study of fluid flow and weld penetration in stationary arc welds using a steady-state two-dimensional finite difference model. The buoyancy force, the electromagnetic force, and the surface tension at the weld pool surface were considered as three driving forces for fluid flow in the model. Later, Kou and Wang[9,10] extended the previous work of Kou and Sun to three dimensions for the case of a moving workpiece beneath a fixed laser beam. They found that surface tension significantly affects both convection and weld pool penetration in laser generated pools. However, in both studies the welding model assumes a flat free surface and utilizes the Boussinesq approximation to simplify the governing equations.

Both Zacharia *et al.*[11] and Paul and Debroy[12] concentrated their efforts on describing free surface effects during laser welding. In both papers they compared their finite difference model to experimental measurements and found that the computed surface topography and the observed surface topography agreed well. In a later study, Zacharia *et al.*[13] developed a computer simulation utilizing discrete element analysis (DEA) for describing transient three-dimensional convection and conduction heat transfer in both moving and stationary arc welding processes. This mathematical formulation, free of the Boussinesq approximation, included the effects of buoyancy, electromagnetic and surface tension driving forces and treated the weld pool as a truly deformable free surface. According to the study, they concluded that surface tension is the controlling force dominating convection in the weld pool. Subsequently, Zacharia *et al.*[14] conducted a systematic study to verify the results of a transient multidimensional computational model with observed results in an experimental study. In addition, Zacharia *et al.*[15] studied the effects of weld pool evaporation and temperature dependent material properties on a developing well pool. Their results indicate temperature dependent material properties should be included in numerical and physical models describing welding, and they concluded that vapourization effects significantly alter the development of the weld pool and should not be neglected.

In a previous paper, Olson and Thomazin[16] applied finite element techniques to analyze laser welding of metals and ceramics. Their planar model employed a full two-dimensional steady form of the conservation equations rather than the Boussinesq approximation and included a flat free surface. The results indicated that convective energy transport is substantially more significant in ceramics than in metals.

In this paper, analysis concerning the differences between ceramic and metallic laser welding will be examined using an axisymmetric numerical formulation. As in the previous study[16], a flat free surface is assumed and temperature dependent material properties are incorporated into the finite element model.

GOVERNING EQUATIONS AND BOUNDARY CONDITIONS

The physical geometry under consideration is provided in *Figure 1*. For this spot welding mode, the laser flux is Gaussian in nature and the sides of the workpiece are maintained at ambient temperature while the bottom surface is considered insulated.

The differential equations govenining fluid motion and heat transfer for the axisymmetric geometry under consideration are the steady two-dimensional conservation equations[17,18,19],

Mass

$$(\rho u)_{,r}+(\rho w)_{,z}+\frac{\rho u}{r}=0 \tag{1}$$

r-momentum

$$u(\rho u)_{,r}+w(\rho u)_{,z}+\rho u\left(u_{,r}+w_{,z}+\frac{u}{r}\right)=-P_{,r}+\frac{2}{r}(r\mu u_{,r})_{,r}+(\mu(u_{,z}+w_{,r}))_{,z} \tag{2}$$

z-momentum

$$u(\rho w)_{,r}+w(\rho w)_{,z}+\rho w\left(u_{,r}+w_{,z}+\frac{u}{r}\right)=-P_{,z}+\rho g+\frac{1}{r}(r\mu(u_{,z}+w_{,r}))_{,r}+2(\mu w_{,z})_{,z} \tag{3}$$

Energy equation

$$u(\rho h)_{,r}+w(\rho h)_{,z}+\rho h\left(u_{,r}+w_{,z}+\frac{u}{r}\right)=uP_{,r}+wP_{,z}+\frac{1}{r}(rkT_{,r})_{,r}+(kT_{,z})_{,z}+\Phi \tag{4}$$

where

r = radial coordinate
z = axial coordinate
u = velocity in radial direction
w = velocity in axial direction
ρ = density
μ = first coefficient of viscosity
g = gravitational constant
P = pressure
h = specific enthalpy
T = temperature
k = thermal conductivity

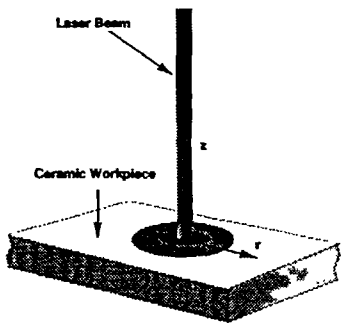

Figure 1 Geometry for axisymmetric welding

and the comma denotes differentiation ($u_{,r}=\partial u/\partial r$). The last term in Equation (4) is the dissipation function: $\Phi=\mu[2(u_{,r}^2+w_{,z}^2+(u/r)^2)+(u_{,z}+w_{,r})^2]$. However, it is considered negligible for this analysis. In the momentum equations, the viscous stresses were assumed to be adequately represented by a Newtonian fluid where μ is the first coefficient of viscosity and the second coefficient of viscosity was assumed to be zero. The material properties ρ, k, μ and h are assumed to be known functions of temperature leaving the unknowns in the governing equations as temperature, pressure and velocities. Additionally, the solid region of the workpiece will simply be treated as a fluid with a large viscosity, a method used successfully in modelling attempts by Kou *et al.*[8,9,10].

The region between the liquidus and solidus temperatures is commonly called the mushy zone. This region contains both liquid and solid phases of the material where the liquid is contained within the solid matrix. Although the finite element model developed here can treat arbitrary (piecewise linear) temperature variations of material properties, accurate data for material properties is difficult to obtain. In the mushy zone, the thermal conductivity, enthalpy, density and viscosity were modelled as linear functions of temperature. Outside the mushy zone thermal conductivity and viscosity were modelled as constant functions while enthalpy and density were modelled as linear functions.

The surface tension effects on a free surface can increase the rate at which energy is transported and have been found to be a dominant force in driving fluid in a melted pool. Generally, two stress boundary conditions on the liquid surface must be satisfied[20],

$$n_i(-P\delta_{ij}+\tau_{ij})n_j=\gamma\kappa \tag{5}$$

and

$$t_i\tau_{ij}n_j=(t_i\gamma)_{,i} \tag{6}$$

where n_i is the outward unit normal, κ is twice the curvatuve, t_i is any tangent vector and γ is the surface tension. However, in our analyses we will assume a flat free surface, so (5) is replaced by $w=0$. In the flat axisymmetric case, (6) reduces to the Marangoni effect term,

$$\mu u_{,z}=-\gamma_{,r}. \tag{7}$$

FINITE ELEMENT FORMULATION

As in the usual Galerkin method, the governing equations (1, 2, 3, 4) are premultiplied by weighting functions ($\bar{u}$, $\bar{w}$, $\bar{P}$, $\bar{T}$) and are integrated over the computational domain[21,22,23],

Mass

$$\int_V \bar{P}\left[(\rho u)_{,r}+(\rho w)_{,z}+\frac{\rho u}{r}\right]\mathrm{d}V=0 \tag{8}$$

r-momentum

$$\int_V \left\{\bar{u}\left[u(\rho u)_{,r}+w(\rho u)_{,z}+\rho u\left(u_{,r}+w_{,z}+\frac{u}{r}\right)\right]-P\bar{u}_{,r}-\frac{P\bar{u}}{r}+2\mu u_{,r}\bar{u}_{,r}+\mu(u_{,z}+w_{,r})\bar{u}_{,z}\right\}\mathrm{d}V$$
$$=\int_S[(-P+2\mu u_{,r})n_r+\mu(u_{,z}+w_{,r})n_z]\bar{u}\,\mathrm{d}S \tag{9}$$

z-momentum

$$\int_V \left\{\bar{w}\left[u(\rho w)_{,r}+w(\rho w)_{,z}+\rho w\left(u_{,r}+w_{,z}+\frac{u}{r}\right)\right]-P\bar{w}_{,z}+\rho g\bar{w}+\mu(u_{,z}+w_{,r})\bar{w}_{,r}+2\mu w_{,z}\bar{w}_{,z}\right\}\mathrm{d}V$$
$$=\int_S[\mu(u_{,z}+w_{,r})n_r+(-P+2\mu w_{,z})n_z]\bar{w}\,\mathrm{d}S \tag{10}$$

Energy equation

$$\int_V \left\{ \bar{T}\left[u(\rho h)_{,r} + w(\rho h)_{,z} + \rho h\left(u_{,r} + w_{,z} + \frac{u}{r} \right) - uP_{,r} - wP_{,z} \right] + kT_{,r}\bar{T}_{,r} + kT_{,z}\bar{T}_{,z} \right\} \mathrm{d}V = \int_S (kT_{,r}n_r + kT_{,z}n_z)\bar{T}\,\mathrm{d}S \quad (11)$$

where $\mathrm{d}V \equiv 2\pi r\,\mathrm{d}r\,\mathrm{d}z$ and n_r, n_z are the components of the unit normal vector to the surface.

Ho and Patera[20] show that the surface stress integral in (9) and (10) can be written in terms of the surface tension as,

$$\int_S \gamma g_i^z \bar{u}_{i,\alpha}\,\mathrm{d}S. \quad (12)$$

The definition of the new terms are provided in Appendix A. Equation (12) generalizes Ruschak's[24] variational formulation for three dimensions and includes the Marangoni effect caused by temperature dependent surface tension.

The standard isoparametric finite element interpolations were used for all variables. Velocities and temperatures were interpolated using a 9-node element with C^0 continuity and pressures were interpolated linearly with C^{-1} continuity (i.e. 3 pressure unknowns in each element with discontinuous pressure interpolations).

Standard finite element techniques[21] were used to solve the governing equations. The weak forms appearing in (8) through (11) were used to build a set of discrete global residual equations, which were then solved using a modified Newton-Raphson algorithm.

VERIFICATION

To verify the program analysis results a number of standard test cases were examined as well as a system similar to the axisymmetric spot welding case of Ramanan and Korpela[6,7]. The finite element mesh for the physical system investigated by Ramanan and Korpela is provided in *Figure 2*. Below the laser flux the fluid is driven by surface tension and the laser is modelled as an exponentially decaying energy source. The mesh was refined in the liquid region below the laser flux to capture regions of high velocity and shear and made coarser in the solid region away from the laser flux.

In discussing the results, dimensionless groups Ramanan and Korpela[7] established in their axisymmetric laser welding model were adopted in our model. They studied steady state welding and considered coupled fluid flow and heat transfer in the weld pool. Both variable surface tension and buoyancy effects were included in their model, but they did neglect latent heat effects.

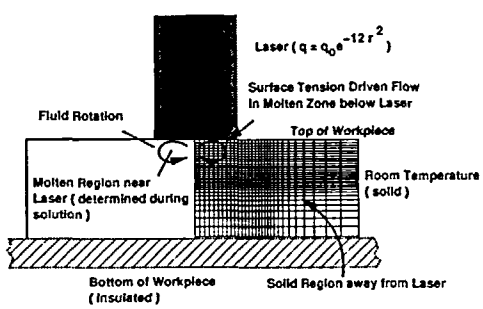

Figure 2 Geometry and finite element mesh for axisymmetric spot welding

The adopted dimensionless groups include,

$$Re=\frac{\rho_l UL}{\mu_l} \tag{13}$$

$$Pr=\frac{c_p\mu_l}{k_l} \tag{14}$$

and

$$Gr=\frac{\rho_l^2 g\beta\,\Delta TL^3}{\mu_l^2} \tag{15}$$

where the characteristic velocity and temperature are given by,

$$U=\frac{\partial\gamma}{\partial T}\frac{\Delta T}{\mu_l}\frac{h}{L} \tag{16}$$

and

$$\Delta T=\frac{\overline{q_0}L}{k_l} \tag{17}$$

respectively. The workpiece height, workpiece length, and characteristic heat flux absorbed at the surface are defined as h, L and $\overline{q_0}$, respectively, and the subscript l on the material properties denotes the liquid state. Notice that both the characteristic velocity and temperature must be inferred from the other parameters in the problem. For their aluminum welding cases, Ramanan and Korpela used $Gr=2.3\times10^6$ and $Pr=0.01$. They employed a dimensionless ambient temperature $T_A^*=-0.42$, solidus temperature $T_s^*=-0.047$, liquidus temperature $T_l^*=0$, and a conductivity ratio $k_l/k_s=0.643$. In dimensionless terms, the surface heat flux from the laser is givey by $q=q_0\,e^{-12r^2}$. They computed velocity and temperature profiles for $Re=10{,}600$, 42,500 and 200,000.

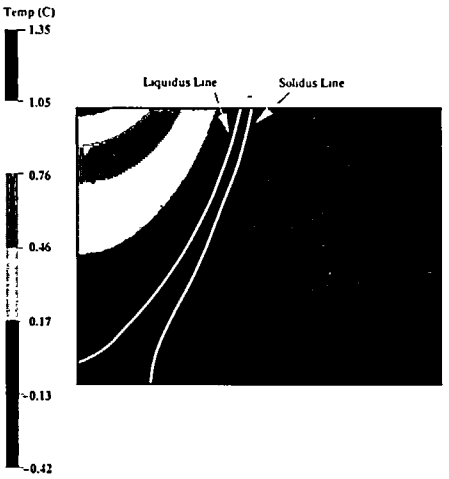

Figure 3 Dimensionless temperature profiles for aluminum laser welding, fluid flow ignored

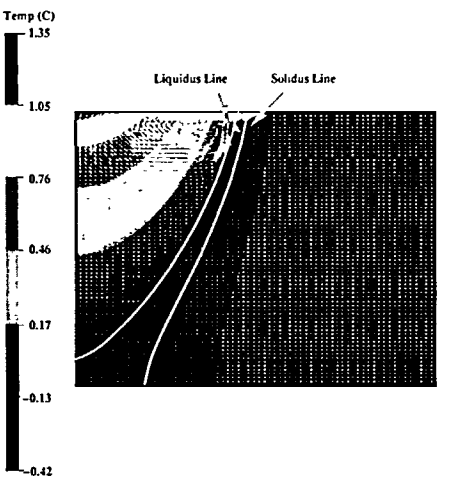

Figure 4 Dimensionless temperature and velocity profiles for aluminum laser welding with $Re=10^4$, $Ge=2.3\times10^6$ and $Pr=0.01$

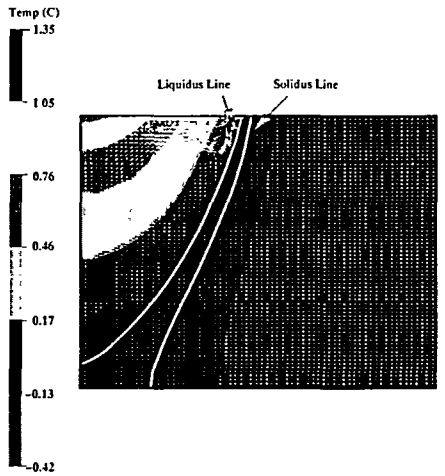

Figure 5 Dimensionless temperature and velocity profiles for aluminum laser welding with $Re=5\times10^4$, $Ge=2.3\times10^6$ and $Pr=0.01$

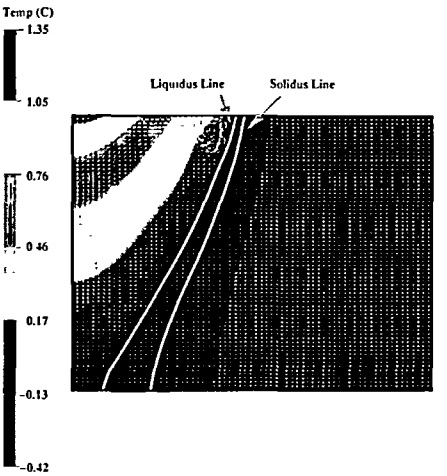

Figure 6 Dimensionless temperature and velocity profiles for aluminum laser welding with $Re=2\times10^5$, $Ge=2.3\times10^6$ and $Pr=0.01$

We examined several aluminum laser welding cases with our modelling techniques with $Gr=2.3\times10^6$ and $Pr=0.01$. The plot for the pure conduction case is shown in *Figure 3*. (This is the result when fluid flow effects are completely ignored.) The plot for $Re=10^4$ is provided in *Figure 4*. The circulation zone for $Re=10^4$ occupies a large portion of the liquidus region, yet when comparing the conduction solution to the coupled heat and fluid flow the thermal profile is only slightly affected. The plots for $Re=5\times10^4$ and $Re=2\times10^5$ are given in *Figures 5* and *6*, respectively. Notice that as the Reynolds number is increased the circulation zone migrates to the outer edge of the liquidus pool. For the low Reynolds number cases the liquidus line ends on the centreline of the workpiece, but at the highest Reynolds number this line has moved to the bottom. However, when the thermal profile is compared for these different cases the thermal profile changes little even at higher Reynolds number flows. This phenomenon indicates the thermal energy is simply diffused rather than convectively redistributed for this welding mode. Physically, one should expect this behaviour for liquid metals, since $Pr\ll1$, an indication the energy diffusion rate dominates the momentum diffusion rate. We also observe that the nondimensional surface velocities decrease with increasing Reynolds number, due to the nature of the nondimensionalization chosen. These results are all consistent with the results obtained by Ramanan and Korpela[7] in their studies of axisymmetric spot welding.

RESULTS FOR CERAMIC AND METALS WELDING

The dimensionless results reported in the previous section compare well with previously reported results. However, in analyzing aluminum and alumina welding we chose to use dimensional variables to aid in the physical interpretration of the results.

The dimensionless material properties listed in *Table 1* were used for modelling the aluminum and alumina. The values for aluminum were based upon data from Kou and Wang[9], and are the dimensional values associated with the dimensionless groups from our verification section. Obtaining data typical of ceramics such as aluminum (Al_2O_3) is more difficult; however, critical values for a number of parameters are provided in *Table 1*. There are several differences between the two laser welding cases which should be apparent. Notice in *Table 1* the surface tension temperature coefficient, $(\partial\gamma/\partial T)$, for aluminum is roughly six times larger than the surface tension temperature coefficient of aluminum. Also, the heat flux for metal corresponds to an absorbed power of 1900 Watts on the part surface, yet the mean laser flux for alumina is only one-seventh

Table 1 Dimensional welding parameters for aluminum and alumina. (Key: [1] = Kou and Wang, 1986b, [2] = Ramanan and Korpela, 1990a, [3] = Bates *et al.*, 1971, [4] = Wilcox *et al.*, 1977, [5] = Kingery *et al.*, 1976, [6] = Cox *et al.*, 1989, [7] = Rosenberger, 1979, [8] = Goldsmith *et al.*, 1961)

Property	Aluminum (metal)	Alumina (ceramic)
β (/C)	10^{-4} [1]	3.8×10^{-4} [3]
$\partial\gamma/\partial Y$ (kg/s^{2}C)	-0.35×10^{-3} [1]	-6×10^{-5} [4]
T_l (C)	652 [1]	2054 [5]
T_s (C)	582 [1]	1828 [5]
T_A (C)	25 [1]	25
ρ_l (kg/m^3)	2700 [1]	3000 [3]
ρ_s (kg/m^3)	2700 [1]	3000
$c_{P,l}$ (J/kgC)	1066 [1]	1600 [6]
$c_{P,s}$ (J/kgC)	1066 [1]	1300 [6]
k_L (W/mC)	108 [1]	4.8 [7]
k_S (W/mC)	168 [1]	5.44 [8]
μ_l (kg/ms)	10^{-3} [1]	0.105 [7]
μ_s (kg/ms)	10^5 [1]	0.105×10^3
q_0 (W/m^2)	2.0×10^8 [2]	2.9×10^7
h (m)	3×10^{-3} [2]	3×10^{-3}
L (m)	6×10^{-3} [2]	6×10^{-3}

Table 2 Dimensionless welding parameters for aluminum and alumina

Dimensionless property	Aluminum (metal)	Alumina (ceramic)
T_A^*	−0.42	−0.4228
T_s^*	−0.047	−0.0472
T_l^*	0.0	0.0
k_l/k_s	0.643	0.88
Pr	0.01	35
Gr	2.3×10^6	3.14×10^3
Re	2×10^5	234

of the laser flux for aluminum. (The surface heat flux was $q = q_0\, e^{-\alpha r^2/L^2}$, with $\alpha = 12$.) The reduction of the laser flux was necessary to keep the alumina weld pool comparable in size to the aluminum weld pool, and is due to the low conductivity of the ceramic combined with its high melting temperature.

Table 2 compares the dimensionless groups for the aluminum and alumina. Here the most striking differences are in the Prandtl number, which is 3500 times larger for the ceramic, and the Reynolds number, which is orders of magnitude less for the ceramic. Hence we would expect a more viscous flow in the ceramic, with closer coupling between the fluid flow and heat transfer.

Dimensional results for $Re = 200{,}000$ aluminum welding are shown in *Figure 7*. The top plot shows the conduction only solution and the bottom plot is combined heat and fluid flow. The maximum temperature in the molten pool is 2396 C with fluid flow, and 2406 C when fluid flow is ignored. As indicated previously, the weld pool boundaries are not significantly affected by the fluid flow. *Figure 8* shows the finite element mesh superimposed on the thermal profile, and indicates the regions of substantial refinement near the mushy zone.

Employing the alumina material properties produces the results provided in *Figure 9*. Once again the top plot is the conduction only solution and the bottom plot is combined heat and

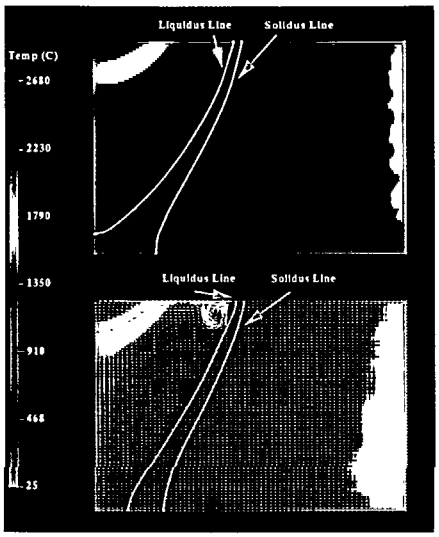

Figure 7 Temperature and velocity profiles for aluminum laser welding with $Re = 2 \times 10^5$. (Top plot: conduction only. Bottom plot: combined heat and fluid flow.)

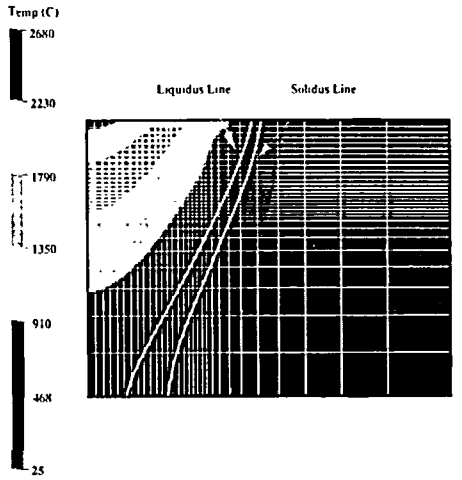

Figure 8 Finite element mesh for aluminum laser welding. (Mesh superimposed on thermal profile for $Re = 2 \times 10^5$.)

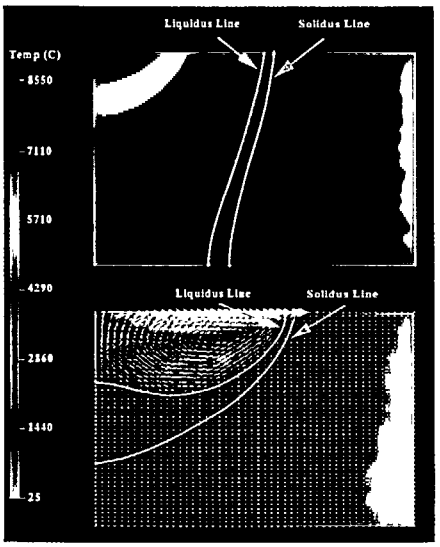

Figure 9 Temperature and velocity profiles for alumina laser welding with $Re = 234$. (Top plot: conduction only. Bottom plot: combined heat and fluid flow.)

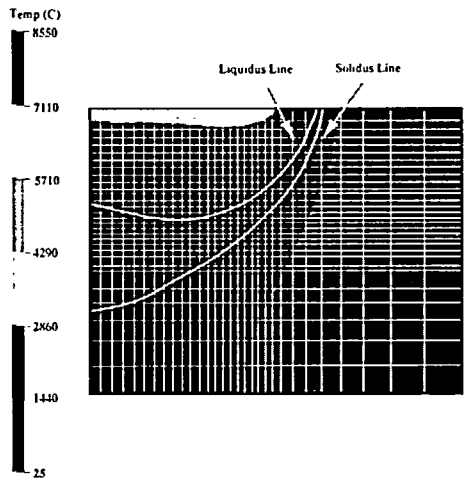

Figure 10 Finite element mesh for alumina laser welding. (Mesh superimposed on thermal profile for $Re = 234$.)

fluid flow. The maximum temperature in the molten pool is 8445 C without fluid flow, and 3463 C with fluid flow. When comparing aluminum and alumina, the coupled heat and fluid flow profiles are quite different. For the alumina case, introduction of fluid motion substantially changes the location of the mushy region whereas for metal the location remains relatively unchanged. (The change in the liquids line from the workpiece centreline to the workpiece base in the aluminum case is due to a small temperature change of only 10 C.) *Figure 10* shows the finite element mesh, which has the same number of elements as the metal case, but the refined regions are located

near the new mushy zone. The dramatic difference in the two welding cases can be attributed to the different Prandtl numbers: 35 for alumina and 0.01 for aluminum. Hence the convective transport of energy is far more significant for alumina. In addition, the fluid flow in the ceramic involves the entire molten region rather than just the corner as in metals. The weld pool indicated by this analysis for the aluminum is very deep and narrow, while the alumina molten zone is shallow and broad. Clearly, the fluid flow has a dramatic effect on the ceramic molten pool geometry and temperatures.

The welding model developed in this analysis is a crude representation of a physical welding process, although it is similar to that used by other researchers in the past and serves well to illuminate the basic differences between ceramic and metals welding. In a real welding situation radiation effects would certainly be significant, especially given the extremely high temperatures reached by ceramics. The free surface in welding operations is rarely flat and deformations can affect the fluid flow and hence the molten pool temperature distribution. Also, latent heat effects have been ignored in the current study. We are currently beginning a comparison between experimental data for steady laser spot welding of ceramics with more detailed numerical calculations.

Further mesh refinement will be necessary for calculating higher Reynolds number flows for metals, and for better resolution of the fluid and heat flow patterns in ceramics. In fact, the 30×30 computational meshes are not quite adequate for quantitative interpretation of the highest Reynolds number results, although qualitative changes in the solution are not expected. The resolution difficulty could be overcome, or at least minimized, by incorporating an Arbitrary Lagrangian-Eulerian (ALE) moving mesh scheme into the solution procedure. We are currently implementing ALE techniques to adjust the mesh to conform to regions of large fluid or thermal gradients.

CONCLUSIONS

A study of the fluid and thermal flow patterns in steady laser spot welding for aluminum and alumina has been conducted using an axisymmetric model. Both buoyancy and surface tension driving forces for fluid flow have been considered in the overall equation solution. The steady differential forms for the mass, momentum, and energy equations have been solved simultaneously using finite element techniques. Very general material properties and geometries can be treated with this approach.

From the calculations, several conclusions may be stated. Due to the ceramic's much higher melting temperature and low conductivity, the absorbed energy flux for alumina is only one-seventh that of aluminum for similar molten pool sizes. It is also likely that the Boussinesq approximation is inappropriate for modelling ceramic materials since the large temperature changes occurring in ceramic welding will produce substantial property variations. More importantly, for low Prandtl numbers such as those found in aluminum the conduction solution for welding gives a close approximation to the temperature profiles obtained by including fluid flow effects. However, due to their much higher Prandtl numbers, the conduction solution for ceramics bears little similarity to the more realistic picture which emerges when both fluid flow and heat transfer are simultaneously considered.

The numerical models presented in this paper are crude representations of actual welding systems, although they employ models similar to those used by other researchers. Future improvements to the model should include radiation/convection boundaries, free surface deformation effects, and latent heat effects. These improvements should allow us to compare with experiments currently underway. Additionally, incorporating an Arbitrary Lagrangian-Eulerian moving mesh algorithm for concentrating the mesh in areas of high thermal and fluid gradients will allow us to improve the resolution of critical physical features without substantially increasing the computational effort required in the solution.

ACKNOWLEDGEMENTS

The authors are grateful to the Center for Electro-Optics at the University of Nebraska-Lincoln for their support for this project.

APPENDIX A

DEFINITION OF TERMS IN SURFACE TENSION INTEGRAL

Ho and Patera[20] give standard definitions which allow easy computation of the surface tension boundary integral contributions, which we include here for completeness. First, the actual coordinates x_i are mapped into a local coordinate system r^α (i.e. the element coordinate system),

$$x_i = X_i(r^\alpha), \tag{18}$$

and then from differential geometry we take the standard defintions,

$$\boldsymbol{g}_\alpha = X_{,\alpha}, \tag{19}$$

$$\boldsymbol{g}_\alpha \cdot \boldsymbol{g}_\beta = g_{\alpha\beta}, \tag{20}$$

$$g_{\alpha\gamma} g^{\gamma\beta} = \delta_{\alpha\beta}, \tag{21}$$

$$\boldsymbol{g}^\alpha = g^{\alpha\beta} \boldsymbol{g}_\beta, \tag{22}$$

$$g = \sqrt{\det(g_{\alpha\beta})}, \tag{23}$$

$$\mathrm{d}S = g \, \mathrm{d}r^1 \, \mathrm{d}r^2. \tag{24}$$

These definitions are valid for one dimensional interfaces or two-dimensional interfaces.

REFERENCES

1 Oreper, G. M. and Szekely, J. Heat- and fluid-flow phenomena in weld pools, *J. Fluid Mech.*, **147**, 53–79 (1984)
2 Oreper, G. M., Szekely, J. and Eagar, T. W. The role of transient convection in the melting and solidification in arc weldpools, *Met. Trans. B*, **17B**, 735–744 (1986)
3 Oreper, G. M. and Szekely, J. A comprehensive representation of transient weldpool development in spot welding operations, *Met. Trans. A*, **18A**, 1325–1331 (1987)
4 Oreper, G. M. and Szekely, J. The transient solidification of weld pools, *Int. J. Heat Mass Transfer*, **30**, 2205–2209 (1987)
5 Thompson, M. E. and Szekely, J. The transient behavior of weldpools with a deformed free surface, *Int. J. Heat Mass Transfer*, **32** (6), 1007–1019 (1989)
6 Ramanan, N. and Korpela, S. A. Thermocapillary convection in an axi-symmetric pool, *Computers and Fluids*, **18** (2), 205–215 (1990)
7 Ramanan, N. and Korpela, S. A. Fluid dynamics of a stationary weld pool, *Met. Trans. A*, **21A**, 45–57 (1990)
8 Kou, S. and Sun, D. K. Fluid flow and weld penetration in stationary arc welds, *Met. Trans. A*, **16A**, 203–213 (1985)
9 Kou, S. and Wang, Y. H. Three-dimensional convection in laser melted pools, *Met. Trans. A*, **17A**, 2265–2270 (1986)
10 Kou, S. and Wang, Y. H. Computer simulation of convection in moving arc weld pools, *Met. Trans. A*, **17A**, 2271–2277 (1986)
11 Zacharia, T., David, S. A., Vitek, J. M. and Debroy, T. Heat transfer during nd:yag pulsed laser welding and its effect on solidification structure of austenitic stainless steels, *Met. Trans. A*, **20A**, 957–967 (1989)
12 Paul, A. and Debroy, T. Free surface flow and heat transfer in conduction mode laser welding, *Met. Trans B*, **19B**, 851–858 (1988)
13 Zacharia, T., Eraslan, A. H., Aidun, D. K. and David, S. A. Three-dimensional transient model for arc welding process, *Met. Trans. B*, **20B**, 645–659 (Oct 1989)
14 Zacharia, T., David, S. A., Vitek, J. M. and Kraus, H. G. Computational modeling of stationary gas-tungsten-arc weld pools and comparison to stainless steel 304 experimental results, *Met. Trans. B*, **22B**, 243–256 (1991)
15 Zacharia, Y., David, S. A. and Vitek, J. M. Effect of evaporation and temperature-dependent material properties on weld pool development, *Met. Trans. B*, **22B**, 233–241 (1991)
16 Olson, L. G. and Thomazin, J. A. Laser welding of ceramics and metals: Finite element modelling, *Advanced Comput. Meth. in Material Modelling* (1993)

17 Batchelor, G. K. *An Introduction to Fluid Dynamics*, Cambridge University Press, London (1970)
18 White, F. M. *Viscous Fluid Flow*, McGraw-Hill, Inc., New York (1974)
19 Tritton, D. J. *Physical Fluid Dynamics*, Von Nostrand Reinhold, New York (1979)
20 Ho, L.-W. and Patera, A. T. Variational formulation of three-dimensional viscous free-surface flows: natural imposition of surface tension boundary conditions, *Int. J. Num. Meth. Eng.*, **13**, 691–698 (1991)
21 Bathe, K.-J., *Finite Element Procedures in Engineering Analysis*, Prentice Hall, Englewood Cliffs, NJ (1983)
22 Huebner, K. H. and Thornton, E. A. *The Finite Element Method for Engineers*, John Wiley & Sons, Inc., New York, second ed. (1982)
23 Baker, A. J. *Finite Element Computational Fluid Mechanics*, Hemisphere Publishing Corporation, New York (1983)
24 Ruschak, K. J. A method for incorporating free boundaries with surface tension in finite element fluid-flow simulation, *Int. J. Num. Meth. Eng.*, **15**, 639–648 (1980)
25 Bates, J. L., McNeilly, C. E, and Rasmussen, J. J, *Properties of molten ceramics. Ceramics in Severe Environments.* Kriegel, W. W. and Palmour, H. III, editors. Plenum Press, New York, 1971.
26 Wilcox, W. R. and Lefever, R. A. eds., *Preparation and Properties of Solid State Materials*, Marcel Dekker, Inc, New York, 1977.
27 Kingery, K, Bowen, H. K. and Uhlmann, D. R. *Introduction to Ceramics.* John Wiley and Sons, New York, second ed., 1976.
28 Cox, J. D. Wagman, D. D. and Medvedev, U. A. *CoData Key Values for Thermodynamics.* Hemisphere Publishing Corporation, New York, 1989.
29 Goldsmith, A. Waterman, T. E. and Hirschhorn, H. J. *Handbook of Thermophysical Properties of Solid Materials*, vol. 3: Ceramics, Macmillan Company, New York, 1961.
30 Rosenberger, F. *Fundamentals of Crystal Growth I.* Springer-Verlag, New York, 1979.